https://doi.org/10.1016/j.ijheatmasstransfer.2021.121945

Experimental study on the thermal-hydraulic performance of a fluttering split flag in a channel flow

X.L. Zhong[a], S.C. Fu[a,*], K.C. Chan[a], G. Yang[a], H.H. Qiu[b], Christopher Y.H. Chao[a]

[a]Department of Mechanical Engineering, The University of Hong Kong, Hong Kong, China

[b]Department of Mechanical and Aerospace Engineering, The Hong Kong University of Science and Technology, Hong Kong, China

* Corresponding Author Tel.: +(852) 39102154

E-mail address: scfu@hku.hk

Address: Department of Mechanical Engineering, The University of Hong Kong, Hong Kong, China

Highlights

- Inserting a fluttering flag into a channel enhances its heat dissipation.
- Heat dissipation effect by a split flag is superior to that by a full flag.
- Hydraulic loss of a split flag is lower than that of a full flag.
- A split flag starts flutter at a lower wind speed than a full flag.
- The fluid-structure interaction of a split flag is stronger than that of a full flag.

Abstract

The use of flags as vortex generators inside heat sinks has been successfully demonstrated as a heat transfer enhancement technique. However, their thermal-hydraulic performance is usually diminished by the blocking effect induced by the fluttering phenomenon. To tackle this problem, with the expectation to maximize the fluid mixing while minimizing the pressure drop, we report a simple and direct design by splitting a flag into multiple strips. Flags with different strip widths were compared with a full flag on the performance of pressure drop and heat transfer. A high-speed camera is used to investigate their fluttering motion. A piezoelectric plate is attached to the wall to measure the flag's flutter frequency. The results show that the performance of a flag with multiple strips outperforms that of the full flag for its lower pressure drop and higher heat dissipation effect. The performance of split flag is not linear with the strip number and the optimal way in our study is to split the full flag into 4 strips. The maximum thermal-hydraulic performance factor of the split flag is 1.91, which is 26% higher than that of the full flag. Besides, the split flag starts fluttering at a lower wind velocity. All these results demonstrate that the split strategy of a flag acting as a vortex generator is of great potential for improving the heat sink performance.

Keywords

Heat transfer enhancement, Fluid-structure interaction, Split flags, Thermal-hydraulic performance, Heat sink, Convective heat transfer.

Nomenclature

A_{total}	Total heat transfer area, m^2
D	Hydraulic diameter of the channel, m
f	Friction factor
h	Average heat transfer coefficient, $W\ m^{-2}\ K^{-1}$
k	Air thermal conductivity, $W\ m^{-1}\ K^{-1}$

L	Channel length of the test section, m
Nu	Nusselt number
PZT	Piezoelectric plate
Q_{loss}	Background heat loss, W
Q_{net}	Net dissipated heat, W
Q_{total}	Total input power, W
Re	Reynolds number
T	Temperature, K
w	Strip width, m
ΔP	Pressure drop, Pa
η	Thermal-hydraulic performance factor
μ	Air dynamic viscosity, kg m^{-1} s^{-1}

Subscripts

aug	Augmentation
c	Clean channel
m	Modified channel

1. Introduction

Heat is always generated in almost all electronic and mechanical processes. Heat sink has long been used as an effective device to dissipate heat from a heat source to the surrounding. It is mentioned that current heat sinks sometimes cannot satisfy the cooling demands of some electronic products, thus the fast-growing microelectronic technology would be hindered if the development of heat sink cannot catch up to tackle this issue. Many researchers have been seeking ways to improve the heat transfer performance of heat sinks and this is a never-ending chasing.

Generally, a heat sink uses an extended fin structure to increase the area for heat transfer and further increases the heat transfer coefficient by using a fan or pump to drive the fluid passing through the fin structure. Its cooling capacity is typically limited by the thermal boundary layer on the heated surface and the ineffective thermal mixing of the core flow. Introducing additional turbulence is one of the possible techniques for enhancement [1] and this approach can be further classified into active and passive techniques. Passive techniques usually involve making rough surfaces, extended surfaces or displaying stationary vortex generator inside the channels that disrupt the thermal boundary layer by reducing its thickness [2–6]. Built-in stationary delta winglets as a passive vortex generator have been shown to improve the heat transfer by 2.5 times [7] or the overall heat dissipation rate by 20-35% [8]. However, they cause a significant pressure drop, resulting in a lower overall efficiency due to the increased consumption of electricity to power the fans. Active techniques including surface vibration, fluid vibration and synthetic jets utilizing micro-electro-mechanical systems [9], all of which require external power. Celik et al. [10] demonstrated the thermal enhancement by employing the vortex shedding mechanism from a forced oscillating cylinder. Not only would it be beneficial to the heat transfer efficiency, but it would also reduce the pressure drop. A moderate pressure drop was maintained with 60% of augmentation achieved [11], but it, consumed 300% more mechanical power for oscillation. Moreover, installing a power provision system for oscillation in such a limited space is a challenging issue.

Aeroelastic flutter has been identified as one of the potential approaches for heat sink development [12]. It has been proposed to increase the heat transfer by simply inserting fluttering flags in the cavities of a heat sink. The fluttering action provides a vibration effect like the active techniques mentioned above, but it is self-excited and so, an additional actuator is not required. The effect of flow parameters and flag properties on heat transfer characteristics was examined by placing a flexible flag between parallel plates. It is found that as high as 300% improvement in local heat transfer coefficient can be achieved. Although the flag motion may cause blockage effects inside the channel resulting in an increased pressure drop, a numerical comparison was made between the cases of a stationary cylinder and a cylinder with a fluttering plate [13], and the results showed that the overall efficiency of the fluttering case is still higher than that of the stationary vortex generators regardless the higher average pressure drop generated.

Later, a number of studies that employed fluid-structure interaction of flexible structures [14–17] coupled with heat convection have been published [18–21]. Shi et al.[22] used a thin film behind a cylinder in a channel flow to study the effect of flutter-induced vortex on heat transfer in a numerical way. They found that the vortex shedding strengthens the disruption of the thermal boundary layer, leading to an increase of 90.1% on the Nusselt number (Nu). But the thermal-hydraulic performance factor, the ratio of the heat dissipation augmentation to the increase in flow fiction loss, lies only between 0.75 and 1.06 because of the highly increased pressure drop. Another simulation work conducted by Shoele and Mittal [23] studied the effect of reed inertia and bending stiffness on the flutter amplitude, frequency and mode transition. Finally, they achieved a maximum thermal-hydraulic performance factor of 1.24. Yu et al. [24] investigated the vortex dynamics behind an inverted fluttering flag and studied its thermal enhancement effect in a channel flow. The maximum performance factor in his experiment was only about 0.97. In another experimental study, Wang et al. [25] designed an inhomogeneous stepped agitator to decrease the pressure drop penalty and reached a maximum thermal-hydraulic factor of 1.5. However, the inhomogeneous stepped agitator, which was fabricated using two different thickness of material together, will bring complexity to the manufacturing

process.

Based on the above, adding a flexible vortex generator in the heatsink shows promising enhancement of the heat transfer coefficient, but the overall thermal-hydraulic performance was not so satisfactory due to the increased pressure drop. Seeking ways to keep the heat dissipation augmentation while decreasing the induced pressure drop can further improve the thermal-hydraulic performance and reduce energy cost. Li et al. [26] mentioned that the out-of-phase motions of the flags in the same array could decrease the pressure drop. In their study, two flags were installed on the same flag holder at a certain distance. This inspires us that by shortening the distance to zero, the flags will be reorganized as a single flag split into multiple strips, and the flag-induced pressure drop could be decreased compared to a full flag by the potential out-of-phase motions of the strips. Most recently, Zaw et al. [27] discussed the wind energy harvesting performance of a flexible film consisting of several strips. They found that the strip-like film can be vibrated even under a very weak wind, while the bulk film will not flutter under the same wind. We suppose that it is induced from the out-of-phase motion of the strips, which allows the airflow through the gaps between the strips to disturb the static state of the flag so that the flutter motion can actuate at an earlier velocity. All these suggest that splitting a flag into multiple strips is a potential approach to lower the pressure drop.

Therefore, in this work, we propose a simple and direct passive technique to enhance thermal-hydraulic performance by splitting the flag into multiple strips. This study experimentally investigates the effect of different designs of split flags on the heat transfer enhancement and the induced pressure drop. Four flag designs with the same overall dimensions were tested. Three of them were split into different numbers of equal strips along the flow direction, while the flag lengths of all the strips were the same. We expect to decrease the pressure drop due to the gaps between strips when fluttering, while at least maintaining the heat transfer effect compared to a full flag.

2. Methods

2.1 Experimental setup

As shown in Fig 1 (a), the experimental setup consists of a channel (320 mm × 15 mm × 50 mm) made of acrylic plates with a nozzle attached to the inlet. A uniformly heated copper heating plate (150 mm × 50 mm) was embedded into one sidewall of the channel to model a fin of a heat sink. Fourteen thermocouples were embedded inside the heating plate to ensure a uniform temperature distribution. The temperature signals were captured by the Temperature Input Module (NI 9214). The temperature of thermocouples was calibrated using the polyscience isothermal water circulator with temperature of 0 ℃, 30 ℃, 60 ℃ and 90 ℃. A cantilevered flexible flag was placed in the middle of the test section. The entire setup was thermally insulated using insulating foam. Pressure meters were inserted into the inlet and outlet of the test section. The uniform inlet flow field was provided by a wind tunnel (Armfield C15-10) as shown in Fig 1(b). The airflow velocity was measured by velocimetry (TSI-9565-P-NB). The experiment was conducted under constant room temperature conditions. The temperature of the copper heating plate was controlled by a temperature controller (Digisense TC9100) and the heat dissipation was recorded by a power meter (RSPM 8213) after the steady-state was reached. All parts and components of the experimental setup are listed in Table 1 consisting names, models and accuracies with position number shown in Fig 1(a) and Fig 1(b).

The detailed geometries of the four types of the flag are shown in Fig 1 (c). Sample 1 is the full flag with the dimension of 4 cm by 4 cm, and it is named as the 1-1 flag. Sample 2 is a flag that is split into 2 strips, with the strip width of 2 cm. Sample 2 is named as the 1-2 flag. Similarly, Sample 3 is named as the 1-4 flag and the strip width is 1 cm. Sample 4 is named as the 1-8 flag and the strip width is 0.5 cm. The flags were made of Kapton film with the thickness of 25 μm, Young's modulus of 2.5 Gpa, Poisson ratio of 0.34, material density of 1.42×10^3 kg/m^3.

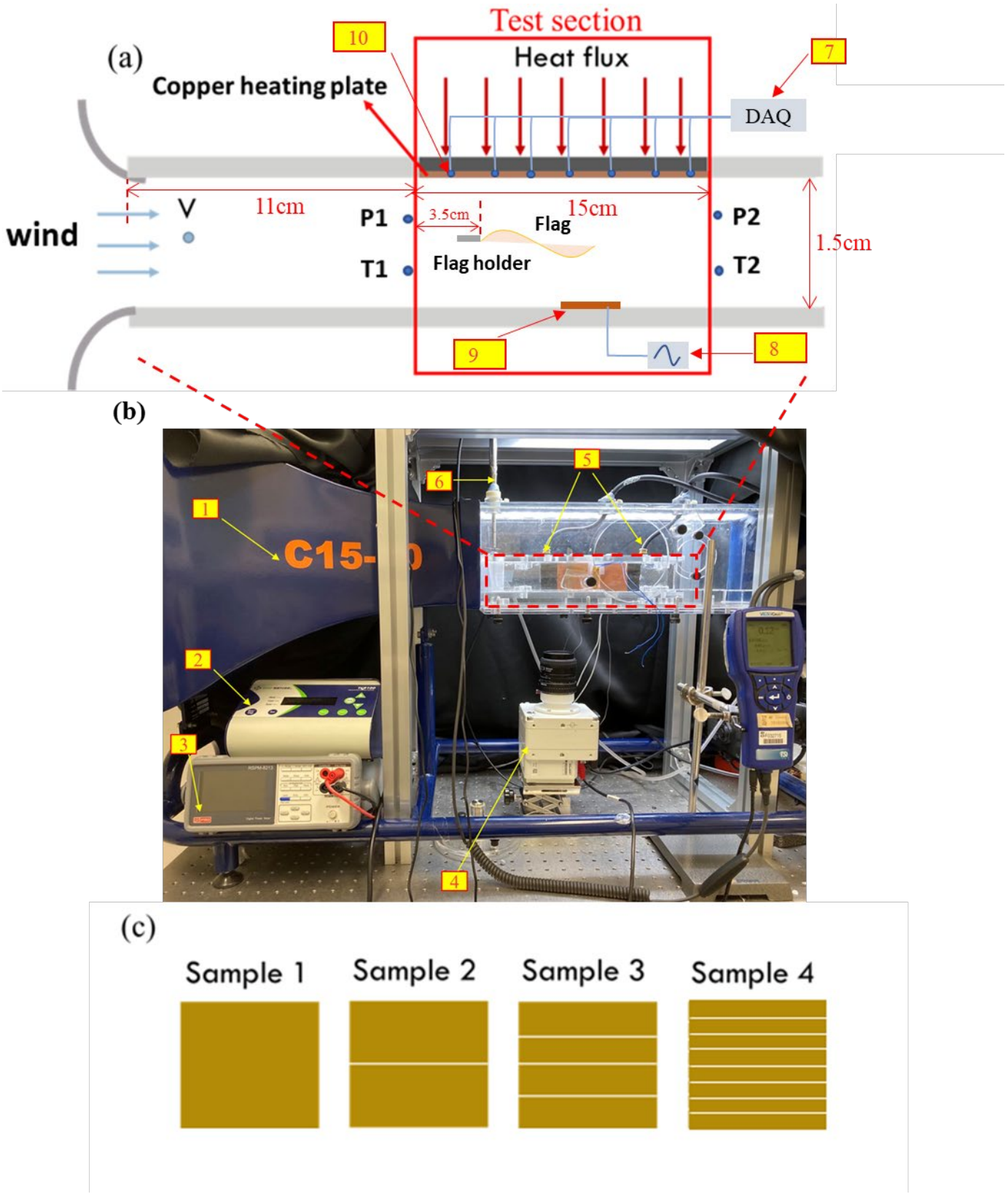

Fig 1 (a) Schematic of the setup; (b) Photography images of the setup; (c) Geometries of the four different types of split flag

Table 1 Components of the experimental setup.

Number	Name	Model	Accuracies
1	Wind tunnel	C15-10, Armfield	/
2	Temperature controller	TC9100, Digi-sense	±0.5 °C
3	Power meter	RSPM-8213, RS-PRO	± (0.1% of reading + 0.1% of range)
4	High speed camera	VEO 410, Phantom	/
5	Pressure meter	9565-P-NB, TSI	±1% of reading
6	Velocity meter	9565-P-NB, TSI	±3% of reading
7	Data logger	9214, National Instruments	±0.37 °C
8	Oscilloscope	TBS 2104, Tektronix	/
9	Piezoelectric plate	M-2807-P1, Smart Material	/
10	Thermocouple	K-type, Omega	±0.37 °C

2.2 Experimental procedure and data analysis

During the experiment, the input power of the heating plate was adjusted to ensure that the temperature difference between the copper heating plate and the inlet air was maintained at 20 K. Time-average input power was recorded for each test under different flow conditions. Before collecting the data, the setup was pre-warmed for around an hour at the lowest wind velocity to assure that the stable heat flux condition was reached. Due to the unavoidable heat conduction between the channel wall and the thermal insulation material, a background test was first conducted at zero wind speed inside the channel while maintaining a 20 K temperature difference to estimate the background heat loss Q_{loss} in the test section.

The net heat dissipation, Q_{net}, is calculated by deducting the background heat loss, Q_{loss}, from the input power of the heating plate, Q_{total}.

$$Q_{\text{net}} = Q_{\text{total}} - Q_{\text{loss}} \tag{1}$$

The Reynolds number of the flow is obtained by the following equation:

$$\text{Re} = \rho U_{\text{air}} D/\mu \tag{2}$$

where ρ is the air density, U_{air} is the air velocity through the channel, D is the hydraulic diameter

of the channel and μ is the air dynamic viscosity. Then, the overall Nusselt number can be calculated by

$$\mathrm{Nu} = hD/k \tag{3}$$

where h is the average heat transfer coefficient and k is the air thermal conductivity. The average heat transfer coefficient was determined by below.

$$h = Q_{\mathrm{net}}/\left(\Delta T_{\mathrm{lmtd}} A_{\mathrm{total}}\right) \tag{4}$$

where A_{total} is the total heat transfer area, ΔT_{lmtd} is the log mean temperature difference between the channel wall temperature and the air flow temperature. Friction factor, f, is calculated by

$$f = 2\Delta PD/(\rho L U_{\mathrm{air}}^2) \tag{5}$$

where ΔP is the streamwise pressure difference between the channel inlet and outlet, and L is the channel length of the test section. For a given Reynolds number, the augmentations of Nusselt number and friction factor were calculated by the equations below respectively.

$$\mathrm{Nu}_{\mathrm{aug}} = \mathrm{Nu}_{\mathrm{m}}/\mathrm{Nu}_{\mathrm{c}} \tag{6}$$

$$f_{\mathrm{aug}} = f_{\mathrm{m}}/f_{\mathrm{c}} \tag{7}$$

where the subscripts m and c represent the modified channel and the clean channel respectively. The thermal-hydraulic performance factor η, is defined to compare the heat transfer enhancement at constant pumping power, i.e, $(\Delta PU_{\mathrm{air}})_{\mathrm{m}}=(\Delta PU_{\mathrm{air}})_{\mathrm{c}}$. This performance factor is calculated as below [26].

$$\eta = (\mathrm{Nu}_{\mathrm{m}}/\mathrm{Nu}_{\mathrm{c}})(f_{\mathrm{m}}/f_{\mathrm{c}})^{-1/3} \tag{8}$$

2.3 Uncertainty analysis

The experimental uncertainty is calculated as below by following the method described in [28].

$$\delta R = \left[\sum_i^N \left(\frac{\partial R}{\partial X_i}\delta X_i\right)^2\right]^{1/2} \tag{9}$$

Each term in Eq. (9) represents the contribution made by the uncertainty of one independent variable, δX_i, to the overall uncertainty in the result, δR. Table 1 shows the measurement accuracies associated with the experimental components. The relative uncertainty is maintained at 3% for the Reynolds number, 5% for the friction factor. The maximum uncertainty for the Nusselt number is less than 2.5%.

2.4 Characterization method

2.4.1 Piezoelectric measurement

To investigate the interaction among strips, flow and channel wall, a piezoelectric plate (PZT) was attached to the channel sidewall to capture the fluttering signal of the strips and then transferred the signal to an oscilloscope (Model TBS2000 with an accuracy of ±3%). The PZT worked as a sensitive strain gauge that transferred the applied deformation (which is highly related to the force imposed on the PZT and the contacting area between the strip and the sidewall) into the voltage signal. A typical raw signal from the oscilloscope is shown in Fig 2(a). Through Fast Fourier Transform (FFT), the raw signal can be transformed to the frequency domain as shown in Fig 2(b). After filtering the background noise and the electronic inherent frequency of 50 Hz, the peak frequency is regarded as the fluttering frequency of the split flag. The fluttering frequency of the example shown in Fig 2(b) is 81.8 Hz. The peak amplitude (1.2V) is also regarded as a sign to evaluate the degree of interaction between the strips and the flow.

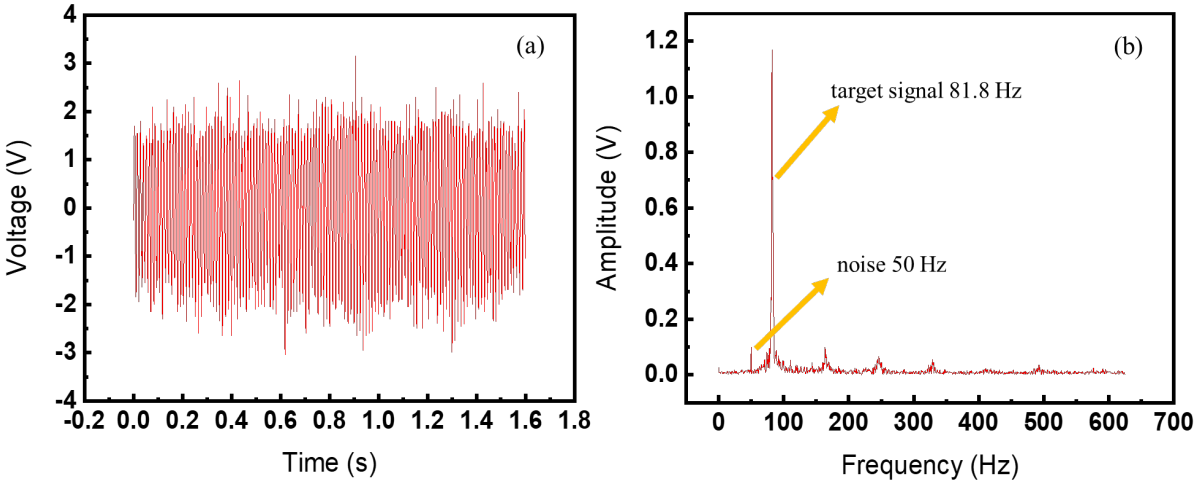

Fig 2 (a) A typical raw signal from the oscilloscope; (b) Data after FFT

2.4.2 High-speed camera investigation

To investigate the fluttering phenomenon of the split flag, the high-speed camera was used to capture the motion of the flag. The surface of the flags was painted black, and the edges were painted white for contrast. The maximum capturing frequency was 1000 Hz. By superimposing frames with a certain time interval from the recorded high-speed video, the fluttering envelope for each case was reconstructed. The amplitude of the flag tip in the direction perpendicular to the channel flow was measured directly in the fluttering envelope. All the process was conducted by software named ImageJ.

3. Results and Discussion

3.1 The effect of splitting the flag on fluttering dynamics

As shown in Fig 3, generally, a fluttering flag, no matter it is a full flag or a split flag, exhibits three fluttering modes with the increasing velocity: static mode, fluttering with increasing amplitude, and fluttering with a restricted amplitude. At a low flow velocity, the flag is static (static mode). At a certain flow velocity, the flag starts fluttering periodically because the aerodynamic and elastic forces destabilize the flag and induce its periodic deformation [29]. The fluttering amplitude gradually increases with the velocity. Until the flag fluttering amplitude is increased to as large as the channel width, the fluttering phenomenon is restricted by the channel wall and the amplitude would not increase any more even with the increasing wind velocity.

The difference between a full flag and a split flag is that for the splitting flag, there exist different fluttering phases for neighboring fluttering strips. This phenomenon is indicated by shadows around the focused strip as highlighted in the yellow rectangles in Fig 3, which represent the positions of other adjacent strips. A specific description is shown in Fig 4, which is a frame from the high-speed video for the split flag. The four strips, which were represented by four white edges, displayed different phases of motion during the interaction with the

channel flow and there are some clearances between them. This out-of-phase fluttering characteristic is supposed to affect the streamwise pressure drop of the channel flow, which will be discussed later.

The fluttering amplitude of different cases is quantitatively measured and compared in Fig 5. The velocity that the flag starts fluttering is recorded as critical velocity [30–32]. The critical velocity can be identified from Fig 5, where the amplitude suddenly has a large jump within a small velocity increment. 1-2 flag shows the lowest critical velocity, followed by 1-4, 1-8, and 1-1 flag. Fig 5 indicates that all the split flags have a lower critical velocity than the full flag.

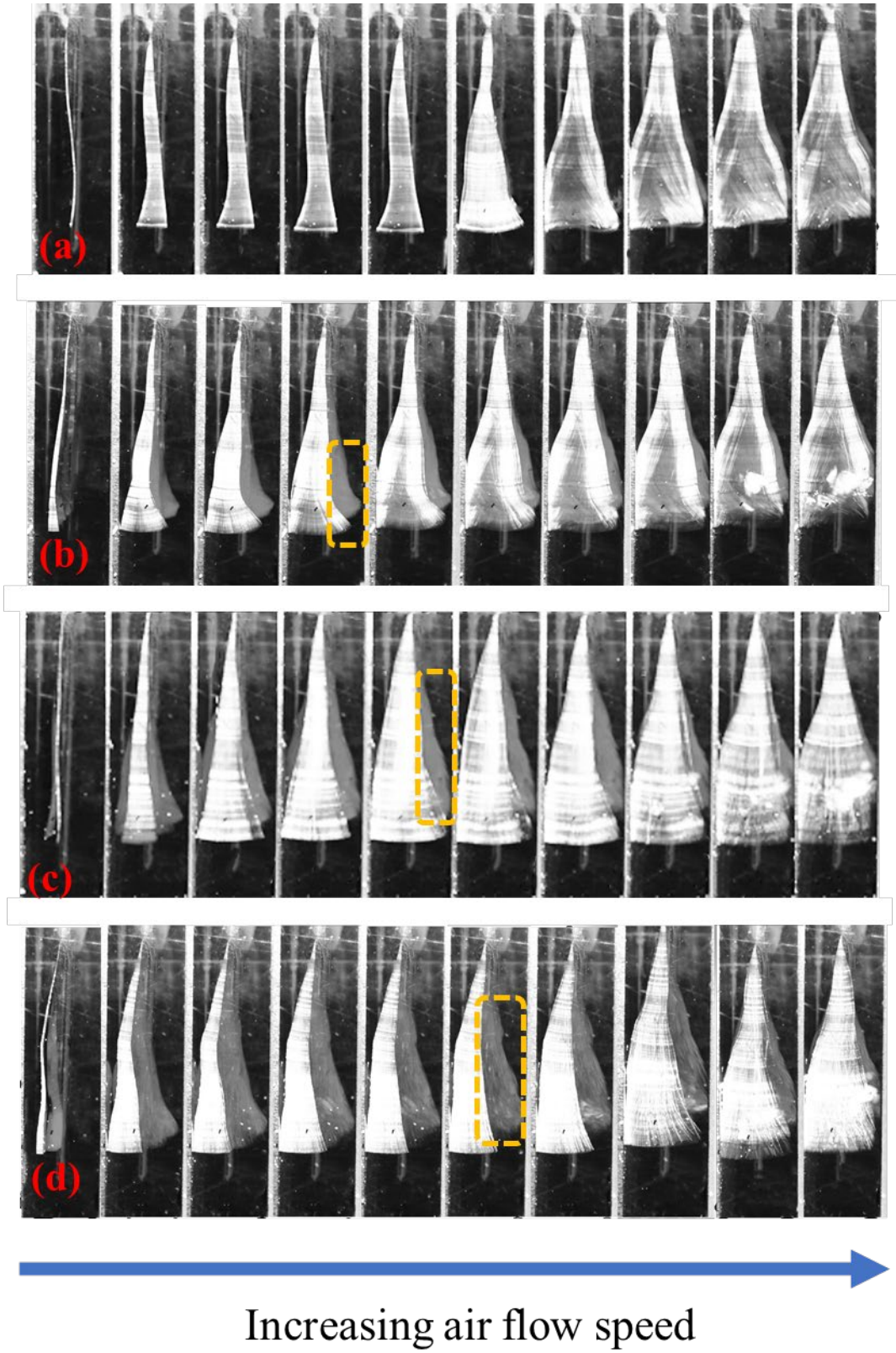

Fig 3 Projection of images of the split flags as a function of increasing airflow velocity for (a) 1-1 flag; (b) 1-2 flag; (c) 1-4 flag; and (d) 1-8 flag. Flow direction is from top to bottom.

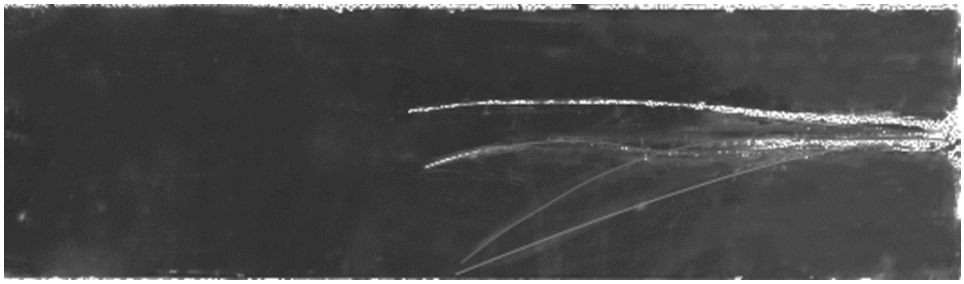

Fig 4 A frame from high-speed video showing the out of phases fluttering motion of the strips for the 1-4 fluttering flag

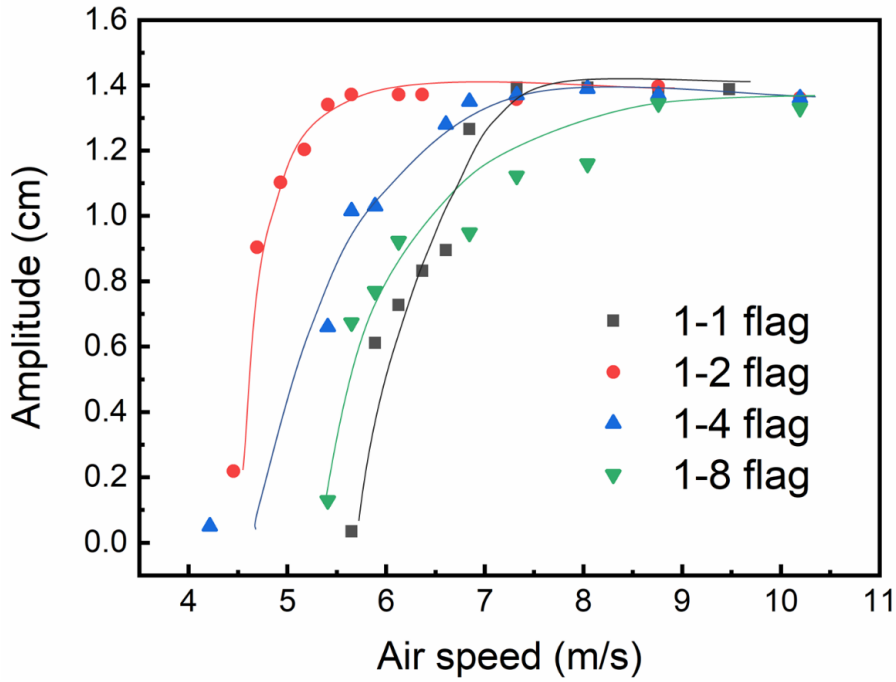

Fig 5 Fluttering amplitudes of split flags

3.2 The effect of splitting the flag on pressure drop

The comparison of pressure drops for different cases is shown in Fig 6(a). The pressure drop for the clean channel (i.e. without flag) increases slowly with the Reynolds number. For the other cases, their pressure drops increase with a larger slope than the clean channel case. This indicates that pressure drop enhances as the flags are installed. Comparing the 4 sample flags, their pressure drops are roughly the same in the low-Re regime, when they have not yet fluttered. With the increase in Reynolds number, they start fluttering and inducing various

amount of friction due to their different interactions with the channel flow: the 1-1 flag always has the highest pressure drop; the 1-8 flag always has the lowest pressure drop; and there is no major difference between the pressure drop of the 1-2 and 1-4 flags. This phenomenon demonstrates that splitting the flag generates a lower pressure drop than the full flag.

Fig 6(b) shows the friction factors of both the clean channel and the channel inserting different flags. For the clean channel case, at the beginning, the friction factor decreases with the increase of Reynolds number. When the Reynolds number greater than 9000, the friction factor appears to level off because the channel flow becomes fully turbulent around this Re. For the channel with flags, the friction factors decrease initially but then increase as the Reynolds number increases, and they are vastly different from the clean channel. The turning point corresponds to the critical velocity where the flag starts flutter. When the flag flutters, the friction factor of the full flag is generally higher than that of the split flags.

Fig 6(c) shows the friction factor augmentation (the ratio between f_m to f_c for a given Reynolds number) against Re. From the onset of flutter, for all the cases, the friction factor augmentation increases as the Reynolds number increases, and the slope gradually decreases with the Reynolds number. Generally, the friction factor augmentation of the full flag is higher than all other splitting cases in the fluttering regime.

All these results demonstrate that the split flags have better performance in reducing hydraulic loss than the full flag. One possible reason is the out of phase fluttering motion of the strips, which leads to gaps between the strips during fluttering. As shown in Fig 7, when air travels through the gaps, the flow blocking effect of the fluttering flag is diminished, thus the streamwise pressure drop decreases. It is also noticed that the 1-8 flag performs the lowest friction factor compared with other flags in the fluttering regime. This may result from the weakened interaction between the slimmer strips, which was measured using the PZT and will be discussed in the next section.

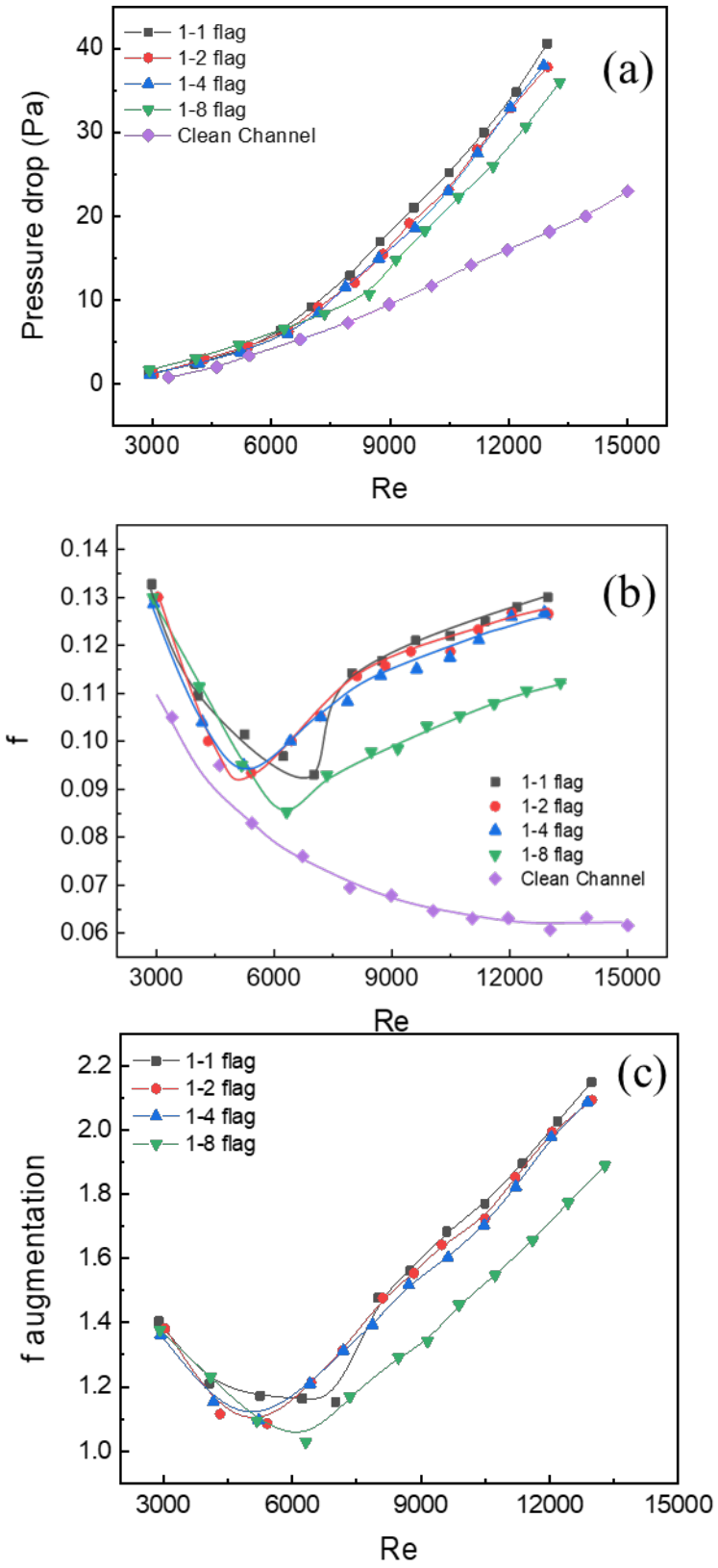

Fig 6 (a) Pressure drop; (b) friction factor; (c) friction augmentation with the increase in Re

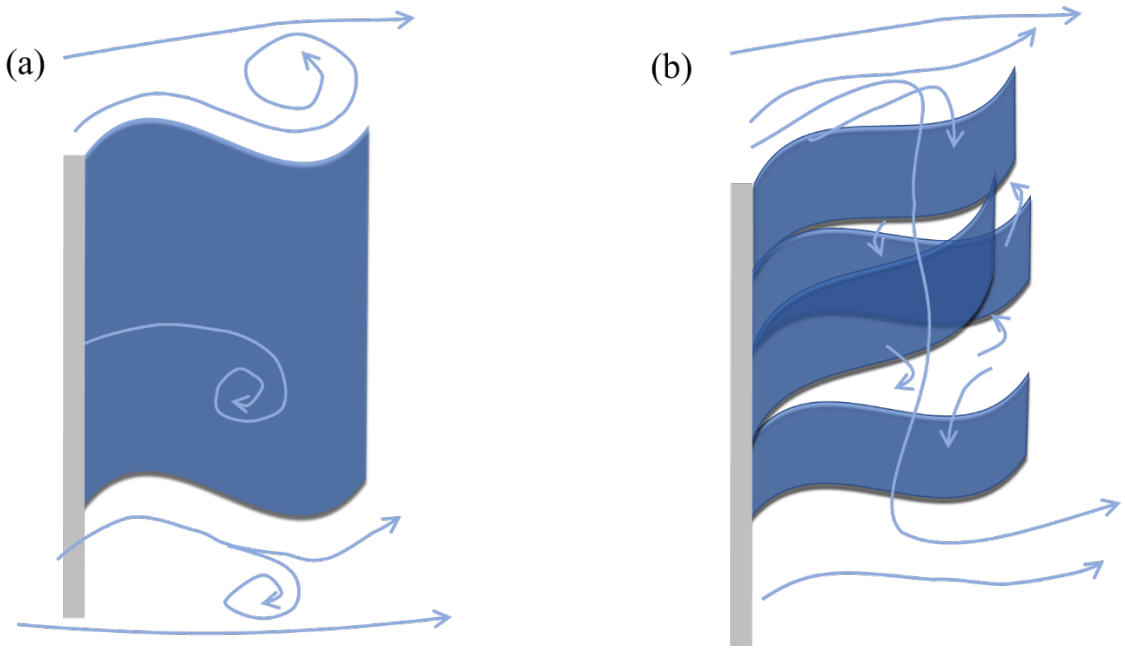

Fig 7 A schematic diagram showing airflow between the strips gaps

3.3 The effect of splitting the flag on heat dissipation

Fig 8(a) shows the relationship between the Nusselt number and the Reynolds number for the clean channel and the channel inserting flags. For the case of clean channel, the Nusselt number increases with the Reynolds number. For the case with flags, when Re < 6000, there is not much difference in Nusselt number between different split flags, while their Nusselt numbers are higher than the case of clean channel. Even when the flags are not yet fluttered, those flags still work as rigid vortex generators thus would slightly enhance the heat transfer.

As the Reynolds number goes higher, for cases with flags, their Nusselt numbers have a large jump in the onset of the fluttering, resulting in a significant enhancement of heat dissipation compared with the case of clean channel. In the fluttering regime, the 1-2 and 1-4 flags have a better heat dissipation effect than the other two cases, while the 1-8 flag shows a surprisingly lower effect than the 1-1 flag. This indicates that the splitting of flag can enhance the heat dissipation effect and the enhancement effect is not linear with the split number, that is, when the flag is split into too many strips, the heat dissipation effect is worse than the full flag. The

result of the 1-4 flag shows the highest Nusselt number of the four flags, showing the existence of the optimum strip width to achieve the best heat transfer effect.

Fig 8(b) shows the Nusselt number augmentation (the ratio of Nu_m to Nu_c for a given Reynolds number). The highest augmented Nusselt numbers for the 1-1, 1-2, 1-4 and 1-8 flags are 2.26, 2.92, 2.98 and 2.42, respectively, and they occur around $7000 < Re < 9000$. When $Re > 9000$, as discussed earlier, the channel flow became fully turbulent and the thermal boundary layer is already very thin, thus further improving the flow mixing does not contribute to a significant heat transfer enhancement. Therefore, the Nusselt number augmentation begins to decrease with the Reynolds number when Re >9000.

The mechanism behind the increase in heat transfer performance at the range of $7000 < Re < 9000$ remains unknown and this attracts us a lot for its best heat dissipation enhancement. To understand how the Nusselt number was affected by the split flags at this regime, the interaction between the strips and the flow was investigated. A PZT was placed on the channel sidewall to capture the fluttering signal of the strips, with the expectation to indicate the degree of interaction of the strips inside the channel flow. Fig 9 presents the frequency of different split flags during fluttering. It indicates that for all the split flags, the frequency increases with the Reynolds number. Higher strips frequency is beneficial for flow mixing and therefore can enhance heat transfer. Besides the fluttering frequency, the amplitude of the signal was also extracted. The signal amplitude is highly related to the strip area and the force at the strip tip when they fluttered. Higher signal amplitude represents stronger interaction between the strips and the flow. As shown in Fig 9(b), the 1-4 flag has the largest signal amplitude, followed by the 1-2, 1-1, and 1-8 flags. This indicates that the degree of interaction is related to the strip width in this study. As the principle of using a flexible vortex generator to enhance heat transfer is the enhanced flow unsteadiness due to fluid-structure interactions [20,33–35], stronger fluid-structure interactions induce better heat dissipation effect in non-fully-turbulent flow. A moderate strip width, which is 1 cm for the 1-4 flag in this study, provides the strongest interaction among all the studied cases, thus leads to the optimal heat dissipation effect. This

well explains the heat transfer performance for the fluttering split flag in the range of 7000 < Re < 9000.

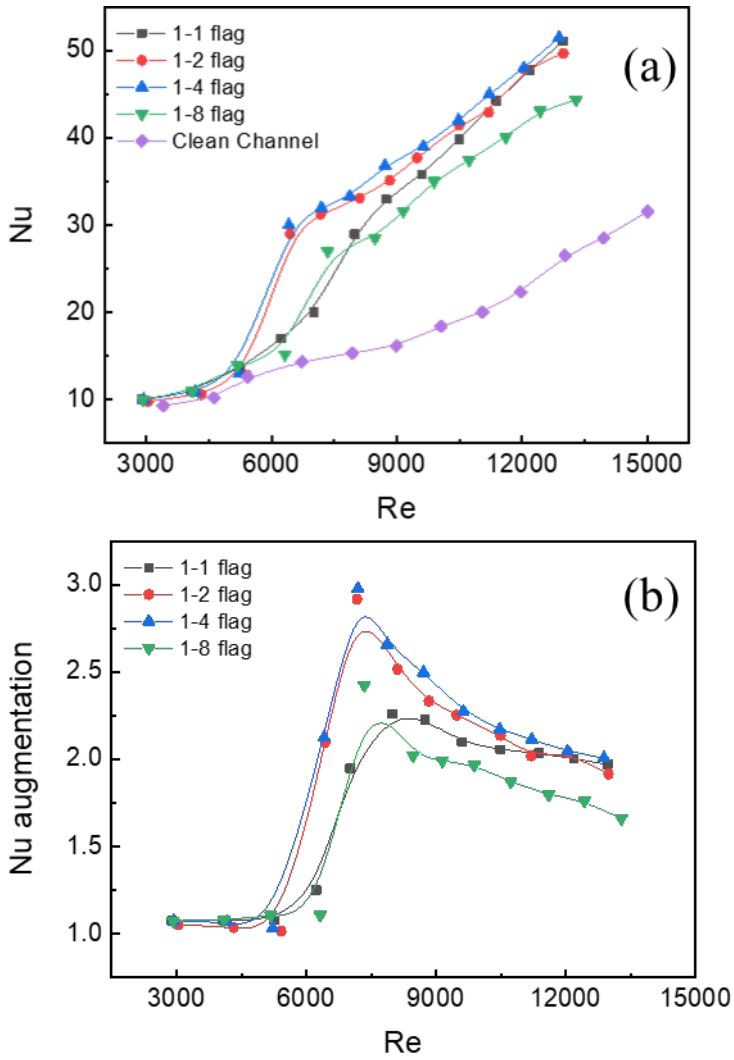

Fig 8 (a)Average Nusselt number and (b) Nu augmentation of the split flags with the increase of Re

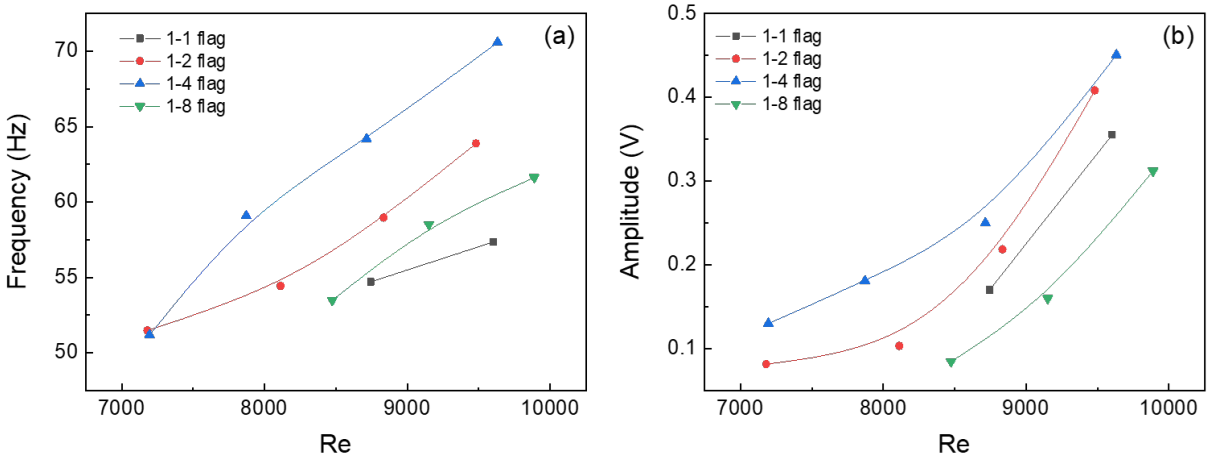

Fig 9 Information from the PZT signal: (a) Frequency; (b) Amplitude

3.4 The effect of splitting the flag on thermal-hydraulic performance

Fig 10 shows the overall thermal-hydraulic performance factor η of the 4 cases. Generally, in the low Reynolds number regime, when the flags have not yet fluttered, η is around 1, which means the heat transfer enhancement brought by the static flag is counteracted by the increased induced friction. The peak η for all the cases happen around the critical velocity, which means that the best performance occurs when the flags just start to flutter. It is because, at that moment, the Nusselt number has a huge jump while the friction just increases moderately. After the peak, as the Reynolds number increases, the η decreases because the heat transfer enhancement greatly decreases due to the thinned boundary layer while the friction gradually increases.

It is also noted that the maximum η is 1.91 for the 1-4 flag, 1.84 for the 1-2 flag, 1.60 for the 1-8 flag, and 1.51 for the 1-1 flag. If the flag is split into too many pieces, it still works to improve flow mixing and decrease the blocking effect comparing to the clean channel. However, comparing to the full flag case, it has not many advantages considering the overall thermal-hydraulic performance. Therefore, the optimum split strategy in this study is to split the full flag into 4 strips.

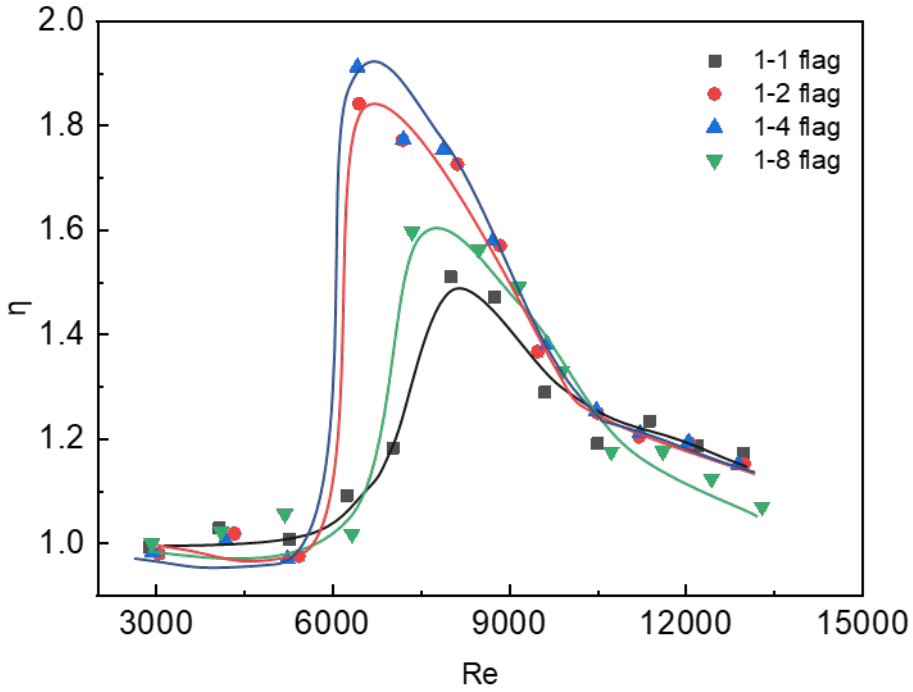

Fig 10 Thermal-hydraulic performance factor

4. Conclusions

In summary, a comprehensive experimental investigation was carried out to explore the thermal-hydraulic performances of flexible flags with multiple strips inserted in a channel. It was found that the split flags started fluttering at a lower wind velocity than the full flag. The pressure drop of the channel flow in the streamwise direction is decreased using the split strategy. The thermal-hydraulic performance of the split flag is better than the full flag. The optimum split strategy in this study is to split the flag into 4 equal strips. The highest thermal-hydraulic performance factor comparing with the clean channel flow is 1.9 for the 1-4 flag, which is 26% higher than that of the full flag. All these results demonstrate that the split strategy is effective with its lower critical velocity, lower hydraulic loss, and higher heat dissipation effect than the full flag, providing guidance for future high-performance heat sinks.

Acknowledgements

This work was supported by the grants from the Research Grants Council of the Hong Kong

Special Administrative Region, China (GRF Project Nos.17205419 & 17203220). The authors would like to thank Mr. Luochang WANG for his technical support and Professor Liqiu WANG for his valuable advice.

References

[1] T.L. Bergman, F.P. Incropera, D.P. DeWitt, A.S. Lavine, Fundamentals of heat and mass transfer, John Wiley & Sons, 2011.

[2] F.A.S. da Silva, D.J. Dezan, A. V Pantaleao, L.O. Salviano, Longitudinal vortex generator applied to heat transfer enhancement of a flat plate solar water heater, Applied Thermal Engineering. 158 (2019) 113790.

[3] Y. Zheng, H. Yang, H. Mazaheri, A. Aghaei, N. Mokhtari, M. Afrand, An investigation on the influence of the shape of the vortex generator on fluid flow and turbulent heat transfer of hybrid nanofluid in a channel, Journal of Thermal Analysis and Calorimetry. 143 (2021) 1425–1438.

[4] M. Samadifar, D. Toghraie, Numerical simulation of heat transfer enhancement in a plate-fin heat exchanger using a new type of vortex generators, Applied Thermal Engineering. 133 (2018) 671–681.

[5] U. Kashyap, K. Das, B.K. Debnath, Effect of surface modification of a rectangular vortex generator on heat transfer rate from a surface to fluid: An extended study, International Journal of Thermal Sciences. 134 (2018) 269–281.

[6] C. Zhai, M.D. Islam, R. Simmons, I. Barsoum, Heat transfer augmentation in a circular tube with delta winglet vortex generator pairs, International Journal of Thermal Sciences. 140 (2019) 480–490.

[7] S. Tiwari, P.L.N. Prasad, G. Biswas, A numerical study of heat transfer in fin- tube heatexchangers using winglet-type vortex generators in common-flow down configuration, Progress in Computational Fluid Dynamics, an International Journal. 3 (2003) 32–41.

[8] M.S. Sohal, Improving Vortex Generators to Enhance the Performance of Air-Cooled Condensers in a Geothermal Power Plant, Idaho National Laboratory (INL), 2005.

[9] R.K.B. Gallegos, R.N. Sharma, Flags as vortex generators for heat transfer enhancement: Gaps and challenges, Renewable and Sustainable Energy Reviews. 76 (2017) 950–962.

[10] B. Celik, M. Raisee, A. Beskok, Heat transfer enhancement in a slot channel via a transversely oscillating adiabatic circular cylinder, International Journal of Heat and Mass Transfer. 53 (2010) 626–634.

[11] A. Beskok, M. Raisee, B. Celik, B. Yagiz, M. Cheraghi, Heat transfer enhancement in a straight channel via a rotationally oscillating adiabatic cylinder, International Journal of Thermal Sciences. 58 (2012) 61–69.

[12] P. Hidalgo, A. Glezer, Small-scale vorticity induced by a self-oscillating fluttering reed for heat transfer augmentation in air cooled heat sinks, in: ASME 2015 International Technical Conference and Exhibition on Packaging and Integration of Electronic and Photonic Microsystems Collocated with the ASME 2015 13th International Conference on Nanochannels, Microchannels, and Minichannels, American Society of Mechanical Engineers Digital Collection, 2015.

[13] A.K. Soti, R. Bhardwaj, J. Sheridan, Flow-induced deformation of a flexible thin structure as manifestation of heat transfer enhancement, International Journal of Heat and Mass Transfer. 84 (2015) 1070–1081.

[14] J. Fu, C. Hefler, H. Qiu, W. Shyy, Effects of aspect ratio on flapping wing aerodynamics

in animal flight, Acta Mechanica Sinica. 30 (2014) 776–786.

[15] K. Shoele, R. Mittal, Flutter instability of a thin flexible plate in a channel, Journal of Fluid Mechanics. 786 (2016) 29–46.

[16] J. Fu, W. Shyy, H. Qiu, Effects of aspect ratio on vortex dynamics of a rotating wing, AIAA Journal. 55 (2017) 4074–4082.

[17] J. Fu, X. Liu, W. Shyy, H. Qiu, Effects of flexibility and aspect ratio on the aerodynamic performance of flapping wings, Bioinspiration & Biomimetics. 13 (2018) 36001.

[18] Y. Chen, Y. Yu, W. Zhou, D. Peng, Y. Liu, Heat transfer enhancement of turbulent channel flow using tandem self-oscillating inverted flags, Physics of Fluids. 30 (2018) 75108.

[19] Y. Chen, Y. Yu, D. Peng, Y. Liu, Heat transfer enhancement of turbulent channel flow using dual self-oscillating inverted flags: Staggered and side-by-side configurations, International Journal of Heat and Mass Transfer. 136 (2019) 851–863.

[20] R.K.B. Gallegos, R.N. Sharma, Heat transfer performance of flag vortex generators in rectangular channels, International Journal of Thermal Sciences. 137 (2019) 26–44.

[21] Z. Li, X. Xu, K. Li, Y. Chen, G. Huang, C.L. Chen, C.H. Chen, A flapping vortex generator for heat transfer enhancement in a rectangular airside fin, International Journal of Heat and Mass Transfer. 118 (2018) 1340–1356.

[22] J. Shi, J. Hu, S.R. Schafer, C.L. Chen, Numerical study of heat transfer enhancement of channel via vortex-induced vibration, Applied Thermal Engineering. 70 (2014) 838–845.

[23] K. Shoele, R. Mittal, Computational study of flow-induced vibration of a reed in a channel and effect on convective heat transfer, Physics of Fluids. 26 (2014) 127103.

[24] Y. Yu, Y. Liu, Y. Chen, Vortex dynamics and heat transfer behind self-oscillating inverted flags of various lengths in channel flow, Physics of Fluids. 30 (2018) 45104.

[25] S. Wang, R. Enyard, K. Li, C.L. Chen, Inverted structurally inhomogeneous stepped agitators in a channel flow, International Journal of Heat and Mass Transfer. 159 (2020) 120094.

[26] K. Li, S. Wang, Z. Ke, C.L. Chen, A novel caudal-fin-inspired hourglass-shaped self-agitator for air-side heat transfer enhancement in plate-fin heat exchanger, Energy Conversion and Management. 187 (2019) 297–315.

[27] N.Y.W. Zaw, H. Roh, I. Kim, T.S. Goh, D. Kim, Omnidirectional triboelectric nanogenerator operated by weak wind towards a self-powered anemoscope, Micromachines. 11 (2020) 414.

[28] R.J. Moffat, Describing the uncertainties in experimental results, Experimental Thermal and Fluid Science. 1 (1988) 3–17.

[29] D. Kim, J. Cossé, C. Cerdeira, M. Gharib, Flapping dynamics of an inverted flag, Journal of Fluid Mechanics. (2013).

[30] M. Argentina, L. Mahadevan, Fluid-flow-induced flutter of a flag, Proceedings of the National Academy of Sciences. 102 (2005) 1829–1834.

[31] C. Eloy, C. Souilliez, L. Schouveiler, Flutter of a rectangular plate, Journal of Fluids and Structures. 23 (2007) 904–919.

[32] C. Eloy, R. Lagrange, C. Souilliez, L. Schouveiler, Aeroelastic instability of cantilevered flexible plates in uniform flow, Journal of Fluid Mechanics. 611 (2008) 97–106.

[33] R.K.B. Gallegos, R.N. Sharma, Flags as vortex generators for heat transfer enhancement:

Gaps and challenges, Renewable and Sustainable Energy Reviews. 76 (2017) 950–962.

[34] A. Rips, K. Shoele, R. Mittal, Heat transfer enhancement in laminar flow heat exchangers due to flapping flags, Physics of Fluids. 32 (2020) 063603.

[35] K. Shoele, R. Mittal, Computational study of flow-induced vibration of a reed in a channel and effect on convective heat transfer, Physics of Fluids. 26 (2014) 127103.